AIAA 82-4189

Supersonic Wing-Body Center of Pressure with Finite Afterbodies

Narendra R. Vira* and Dah-Nien Fan†
Howard University, Washington, D.C.

Nomenclature

$\mathcal{R}$ = wing alone aspect ratio
B = $m\beta$
$(C_{L\alpha})_W$ = lift curve slope for wing alone
C_r = wing root chord
C_t = wing tip chord
D = $\beta d/C_r$
d = body diameter
$K_{B(W)}$ = interference factor for body in the presence of wing
$\bar{K}_{B(W)}$ = $K_{B(W)}(1+\lambda)(s/r-1)\beta(C_{L\alpha})_W$
$L_{B(W)}$ = lift transmitted on the body due to a wing panel
ℓ = length of afterbody
$M_{B(W)}$ = pitching moment at the intersection of wing leading edge and body for two panels
M_∞ = freestream Mach number
m = cotangent of leading edge sweep angle
P = $\ell/\beta d$
q_∞ = freestream dynamic pressure
R = $P+1/D$
r = body radius
s = exposed wing semispan measured from root chord
$\bar{x}$ = center of pressure location of body in the presence of wing measured from the intersection of wing leading edge and body
α = angle of attack
β = $\sqrt{M_\infty^2-1}$
ξ = coordinate along longitudinal axis
η = coordinate along spanwise direction
μ = $\tan^{-1}(\beta)$
λ = wing taper ratio, C_t/C_r

Introduction

THIS Note, a follow-up of Ref. 1, studies the effects of finite-afterbodies on the longitudinal center of pressure location in the presence of a wing, $\bar{x}_{B(W)}$, at supersonic speeds. Closed-form formulas of $\bar{x}_{B(W)}$ for finite afterbodies, more general than those given in Ref. 2 for full/infinite afterbodies, are presented here. Furthermore, $\bar{x}_{B(W)}$ for "negative" afterbodies when the base of the body is forward of the trailing edge of the exposed root chord are determined.

Analysis

The body longitudinal center of pressure location in the presence of wing is[2]

$$\left(\frac{\bar{x}}{C_r}\right)_{B(W)} = \frac{M_{B(W)}}{2L_{B(W)}C_r} = \frac{2\beta}{\alpha q_\infty d C_r^2}\frac{M_{B(W)}}{\bar{K}_{B(W)}} \tag{1}$$

where $M_{B(W)}$ is the pitching moment of the lift carried onto the body by a wing. It can be expressed in double integral as

$$M_{B(W)} = \frac{16q_\infty\alpha B^{3/2}}{\pi\beta(1+B)}\left\{\int_{\eta_1}^{\eta_2} d\eta\int_{\xi_1}^{\xi_2}\xi\left(\frac{\xi/\beta-\eta}{m\xi+\eta}\right)^{1/2}d\xi + \int_{\eta_3}^{\eta_4} d\eta\int_{\xi_3}^{\xi_4}\xi\left(\frac{\xi/\beta-\eta}{m\xi+\eta}\right)^{1/2}d\xi\right\} \tag{2}$$

$$M_{B(W)} = \frac{8q_\infty\alpha m}{\pi(B^2-1)^{1/2}}\left\{\int_{\eta_1}^{\eta_2} d\eta\int_{\xi_1}^{\xi_2}\xi\cos^{-1}\left(\frac{\xi/\beta+m\beta\eta}{\eta+m\xi}\right)d\xi + \int_{\eta_3}^{\eta_4} d\eta\int_{\xi_3}^{\xi_4}\xi\cos^{-1}\left(\frac{\xi/\beta+m\beta\eta}{\eta+m\xi}\right)d\xi\right\} \tag{3}$$

for subsonic and supersonic leading edges, respectively. Closed-form expressions for $\bar{K}_{B(W)}$ in the cases of finite afterbodies were given in Ref. 1. Equations (2) and (3) are restricted to the condition $\mathcal{R}(1+\lambda)(1+B^{-1})\geq 4$ and other assumptions inherent in the formulation of Ref. 2. Limits of integration in the (ξ,η) domain were shown in Fig. 1 of Ref. 1 for two planar models which contain the cases of no-afterbody and full afterbody as special ones.

Again the integrals given in Eqs. (2) and (3) can be evaluated explicitly after some lengthy manipulations. Thus, closed-form expressions for $\bar{x}_{B(W)}$ can be determined.

Results of integration are summarized below for the two planar models mentioned earlier.

Subsonic leading edge ($B<1$)

$$M_{B(W)}(R\leq 1) = \frac{4q_\infty\alpha C_r^3}{\pi\beta^2}\left\{-\frac{4D^2R^2}{3(B+1)B^{1/2}}\left[B^2+\frac{BP}{2R}-\frac{(B+3)P^2}{4R^2}\right]\sqrt{D(BR+P)} + \frac{(B^2+B(B+1)PD)^{1/2}}{9B(B+1)^3}\times[(8B+24)B^2+(14B+6)(B+1)BPD + 3(B-3)(B+1)^2D^2P^2] - \frac{(8B+24)B^3}{9B(B+1)^3} + \frac{4}{3}D^3R^3B^{3/2}\tan^{-1}\left(\frac{1/D}{BR+P}\right)^{1/2} - \frac{(3-B)P^3D^3}{3B}\times\left[\tanh^{-1}\left(\frac{B/D}{BR+P}\right)^{1/2} - \cosh^{-1}\left(\frac{BR+P}{(1+B)P}\right)^{1/2}\right]\right\} \tag{4}$$

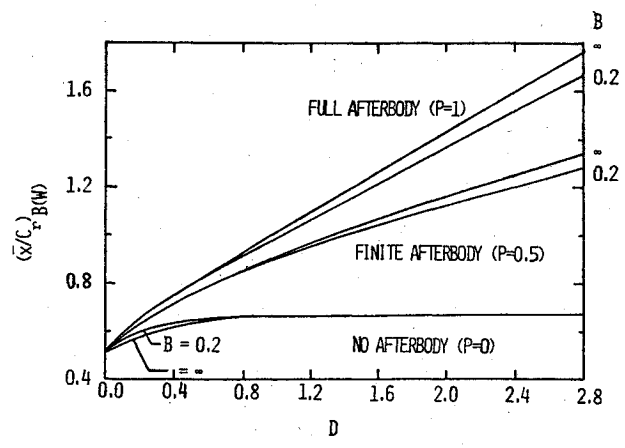

Fig. 1 Center of pressure location on body due to wing as a function of D.

Received Oct. 22, 1981.

*Senior Graduate Research Assistant, Dept. of Mechanical Engineering. Student Member AIAA.
†Professor, Dept. of Mechanical Engineering. Member AIAA.

$$M_{B(W)}(R\geq 1)=M_{B(W)}(R\leq 1)+\frac{4q_\infty\alpha C_r^3}{\pi\beta^2}\left\{\frac{4D^3R^2}{3(1+B)B^{1/2}}\right.$$
$$\times\left[B^2+\frac{B}{2R}-\frac{(B+3)}{4R^2}\right]\sqrt{(R-1)(BR+1)}-\frac{4}{3}D^3R^3B^{3/2}$$
$$\left.\times\tan^{-1}\left(\frac{R-1}{BR+1}\right)^{1/2}+\frac{(3-B)D^3}{3B}\tanh^{-1}\left(\frac{BR-B}{BR+1}\right)^{1/2}\right\} \quad (5)$$

Supersonic leading edge ($B>1$)

$$M_{B(W)}(R\leq 1)=\frac{4q_\infty\alpha mC_r^3}{3\pi\beta}\left\{(1+2DP)^{1/2}\left[\frac{2B+5}{3(1+B)^2}\right.\right.$$
$$\left.+\frac{DP}{3(B+1)}-\frac{D^2P^2}{B}\right]-\frac{2B+5}{3(1+B)^2}+\frac{1}{(B^2-1)^{1/2}}$$
$$\times\left[D^3R^3(1-2B)-\frac{1}{(1+B)^2}-3PD^3R^2\right]\cos^{-1}\left(\frac{R+BP}{BR+P}\right)$$
$$-\frac{1}{(B^2-1)^{1/2}}\left[1-\frac{1}{(1+B)^2}\right]$$
$$\left.\times\cos^{-1}(1/B)+2D^3R^3\cos^{-1}\left(\frac{P}{R}\right)+\frac{P^2D^3}{B}(R^2-P^2)^{1/2}\right\} \quad (6)$$

$$M_{B(W)}(R\geq 1)=M_{B(W)}(R\leq 1)+\frac{4q_\infty\alpha mC_r^3}{3\pi\beta}\left\{\frac{D^3R^3}{(B^2-1)^{1/2}}\right.$$
$$\times\left[2B+\frac{3}{R}-\frac{1}{B^2R^3}\right]\cos^{-1}\left(\frac{B+R}{BR+1}\right)+2D^3R^3$$
$$\left.\times[\sin^{-1}(1/R)-\pi/2]-\frac{D^3}{B}(R^2-1)^{1/2}+\frac{D^3}{B^2}\cosh^{-1}(R)\right\} \quad (7)$$

Equations (4) and (6) are valid for $R\leq 1$, and Eqs. (5) and (7), for $R\geq 1$.

Thus the longitudinal center-of-pressure location under consideration is a function of three independent parameters B, D, and P since R depends on P and D. These parameters were nondimensionalized in accordance with Ref. 2. Numerical results computed from closed-form formulas of $(\bar{x}/C_r)_{B(W)}$ are plotted in Figs. 1 and 2.

It can be seen from Figs. 1 and 2 that the dependence of $(\bar{x}/C_r)_{B(W)}$ on B is very weak. Note that $P=0$ and 1 correspond to, respectively, the cases of no-afterbody and full afterbody (see subsection on Special Cases for detail). Intermediate values of P represent cases of finite afterbody. Furthermore, for given values of B and D, $(\bar{x}/C_r)_{B(W)}$ for finite afterbodies is higher than that obtained by linearly interpolating $(\bar{x}/C_r)_{B(W)}$ for no-afterbody and full afterbody results.

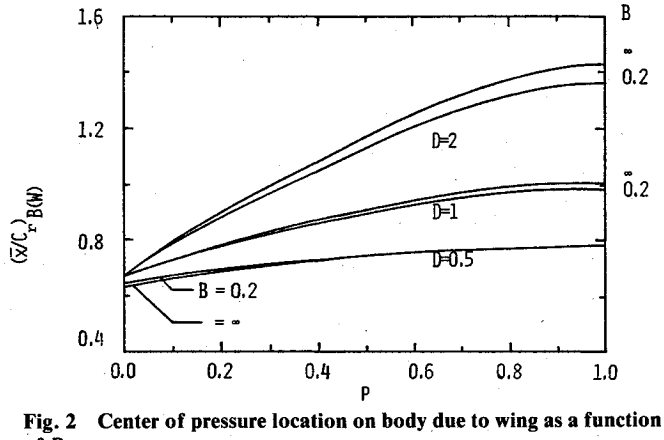

Fig. 2 Center of pressure location on body due to wing as a function of P.

Special Cases

Two special cases will be considered in this section: the case of no-afterbody ($P=0$) and the case of full/infinite afterbody ($P\geq 1$).

No Afterbody

For $P=0$ and $D\geq 1$, Eqs. (4) and (6) reduce to Eqs. (5.3.18) and (5.3.20) of Ref. 3 as they should. For $P=0$ and $D\leq 1$, Eqs. (5) and (7) reduce to Eqs. (5.3.17) and (5.3.19) of Ref. 3, again in full agreement. It should be mentioned that Ref. 2 gives only charts of center of pressure in this case.

Full/Infinite Afterbody

Since $R\geq 1$ when $P=1$, Eqs. (5) and (7), after substituting $P=1$, lead to the same expressions for $(\bar{x}/C_r)_{B(W)}$ in Ref. 2 [Eqs. (67) and (70)]. It is clear that $(\bar{x}/C_r)_{B(W)}(P>1)=(\bar{x}/C_r)_{B(W)}(P=1)$. Equations (4) and (6) are valid only for $R\leq 1$ and should be disregarded for the case of full/infinite afterbody.

"Negative" Afterbody

In the case of negative afterbody, expressions for $(\bar{x}/C_r)_{B(W)}$ can be obtained easily by following the method suggested in Ref. 1. Letting first $P=0$ in Eqs. (4-7) and then replacing D in the resulting expressions by the transformation $D=D_n/(1+P_nD_n)=1/R_n$, $(\bar{x}/C_r)_{B(W)}$ for the planar models under consideration becomes, after dropping the subscript n:

For the subsonic edge

$$\left(\frac{\bar{x}}{C_r}\right)_{B(W)}(0\leq R\leq 1)=\frac{2}{3} \quad (8)$$

$$\left(\frac{\bar{x}}{C_r}\right)_{B(W)}(R\geq 1)=\frac{2}{3}+\frac{32R}{3\pi\bar{K}_{B(W)}(R\geq 1)}$$
$$\times\left\{-B^{3/2}\tan^{-1}\left(\frac{R-1}{BR+1}\right)^{1/2}+\frac{1}{(1+B)RB^{1/2}}\right.$$
$$\times\left[B^2+\frac{B}{2R}-\frac{(B+3)}{4R^2}\right]\sqrt{(R-1)(BR+1)}$$
$$\left.+\frac{(3-B)}{4BR^3}\tanh^{-1}\left(\frac{BR-B}{BR+1}\right)^{1/2}\right\} \quad (9)$$

For the supersonic leading edge

$$\left(\frac{\bar{x}}{C_r}\right)_{B(W)}(0\leq R\leq 1)=\frac{2}{3} \quad (10)$$

$$\left(\frac{\bar{x}}{C_r}\right)_{B(W)}(R\geq 1)=\frac{2}{3}+\frac{8BR}{3\pi\bar{K}_{B(W)}(R\geq 1)}$$
$$\times\left\{2[\sin^{-1}(1/R)-\pi/2]+\frac{1}{(B^2-1)^{1/2}}\right.$$
$$\times[2B+3/R-1/B^2R^3]\cos^{-1}\left(\frac{B+R}{BR+1}\right)$$
$$\left.-\frac{(R^2-1)^{1/2}}{BR^3}+\frac{1}{B^2R^3}\cosh^{-1}(R)\right\} \quad (11)$$

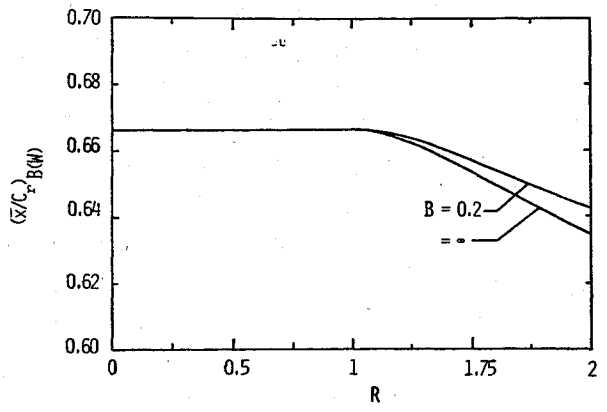

Fig. 3 $(\bar{x}/C_r)_{B(W)}$ **for negative afterbody as a function of** B **and** R.

Obviously $(\bar{x}/C_r)_{B(W)}(R \leq 0) = 0$. Note that $(\bar{x}/C_r)_{B(W)}$ in the case of negative afterbody depends only on the parameters B and R. Variation of $(\bar{x}/C_r)_{B(W)}$ with respect to R and B is illustrated in Fig. 3. The dependence on B is again weak. It is interesting to note that when $0 \leq R \leq 1$, $(\bar{x}/C_r)_{B(W)} = \frac{2}{3}$, a constant. This indicates a proportional variation of the pitching moment with the lift carry on the body by wing [see Eqs. (8) and (10) here and Eqs. (9) and (11) in Ref. 1].

Acknowledgment

Support of this work by NASA Contract NAS 5-24242 to Howard University is hereby gratefully acknowledged. The authors wish to express their thanks to the Technical Officer of contract, Mr. James S. Barrowman, Code 742, at the NASA Goddard Space Flight Center in Greenbelt, Md.

References

[1] Vira, N.R. and Fan, D.N., "Closed-Form Solutions of Supersonic Wing-Body Interference," *AIAA Journal*, Vol. 20, June 1982, pp. 855-857.

[2] Pitts, W.C., Nielsen, J.N., and Kaattari, G.E., "Lift and Center of Pressure of Wing-Body-Tail Combinations at Subsonic, Transonic, and Supersonic Speeds," NASA 1307, 1959.

[3] Fan, D.N. and Vira, N.R., "Aerodynamics of Sounding Rockets," Annual Report to the NASA Goddard Space Flight Center, NASA Contract NAS5-24242, Dept. of Mechanical Engineering, Howard University, Washington, D.C., Oct. 1980.

AIAA 82-4190

Three-Dimensional Shock Structure in a Transonic Flutter Cascade

D. R. Boldman,* A. E. Buggele,† and A. J. Decker‡
NASA Lewis Research Center, Cleveland, Ohio

Introduction

THIS Note describes the results of an exploratory experiment to visualize the transonic shock structure in a linear cascade of two-dimensional airfoils which are externally oscillated in torsion. Since the flowfield contains mixed subsonic-supersonic flow, the supersonic regions can usually be observed with schlieren or shadowgraph systems.[1-2] Although certain information about the shock dynamics can be obtained from high-speed motion pictures of the schlieren images, details concerning the two-dimensionality of the shock during "simulated" flutter are obscure. The present experiment addresses this latter problem through the use of rapid double-pulse holography.[3]

Holographic interferometry has been used for the three-dimensional flow visualization of shock waves in a compressor rotor, e.g., Ref. 4. By comparing holographic and laser anemometer measurements of shock position, it could be seen that blade passage interference fringes caused by motion of the shock wave between the two exposures of a double-exposure hologram, did not always localize on the shock surface. Consequently, it is necessary to analyze and to correct for these fringe localization effects. The results in Ref. 5 indicated that one method of minimizing this fringe localization error is to establish a view of the shock which is close to the tangency at the shock surface. In principle, this condition can readily be realized by observing the flow in a two-dimensional test arrangement such as the flutter cascade used in the present investigation.

Experiment

The flow visualization experiment was performed in a cascade containing three driven biconvex airfoils as shown in Fig. 1. These two-dimensional airfoils had a thickness-to-chord ratio of 0.076, a chord of 7.62 cm, and a span of 9.65 cm. The airfoil chord-to-spacing ratio (solidity) was 1.3. The cascade stagger angle or angle between the flow direction and leading edge plane was 30 deg, typical for transonic rotor blading. Blade-to-blade similarity in shock structure was achieved through adjustable tailboards and a boundary-layer bleed system. The end wall boundary-layer thickness δ measured one chord length upstream of the cascade leading edge was approximately 1 cm.

A modified version of the mechanical drive system described in Ref. 2 was used to oscillate the airfoils. A "simulated" flutter environment was obtained by oscillating the airfoils in harmonic pitching motion about the midchord axis. In this type of motion the instantaneous angle of attack α can be expressed as

$$\alpha = \bar{\alpha}\sin\omega t + \alpha_0$$

The airfoils were driven at a nominal frequency f of 580 Hz, an amplitude $\bar{\alpha}$ of 1.2 deg, and a mean angle of attack α_0 of 6.0 deg. At the freestream Mach number M_∞ of 0.81, the reduced frequency based on the half-chord was about 0.53.

The object beam from a double-pulse ruby laser was transmitted through an optical glass window (cascade end wall) where it passed between the airfoils to the far end wall as shown in Fig. 1. There the light was diffusely reflected by means of a flat-white plastic sheet cemented to the end wall. The diffused light passed back through the airfoils and the optical glass end wall onto a high-resolution photographic plate. Two holograms, separated by a preselected delay time, were recorded on the same plate. In the reconstruction of the double image, interference fringes are formed when there is a slight difference in the refractive index fields between the two exposures. Pulse delay times of 10-20 μs yielded the best images.

Results

Initial tests were performed using the double-pass schlieren flow visualization system described in Ref. 2. The steady-state schlieren image obtained at a mean angle of attack of 6 deg and a Mach number of 0.81 is shown in Fig. 2. This figure clearly reveals a lambda-type shock near the leading edge of

Received Aug. 28, 1981; revision received Dec. 1, 1981. This paper is declared a work of the U.S. Government and therefore is in the public domain.

*Aerospace Engineer. Associate Fellow AIAA.
†Aerospace Engineer. Member AIAA.
‡Optical Physicist.